FreNBRDF: A FREQUENCY-RECTIFIED NEURAL MATERIAL REPRESENTATION

Chenliang Zhou[†], *Zheyuan Hu*[†], *Cengiz Oztireli*

Department of Computer Science and Technology
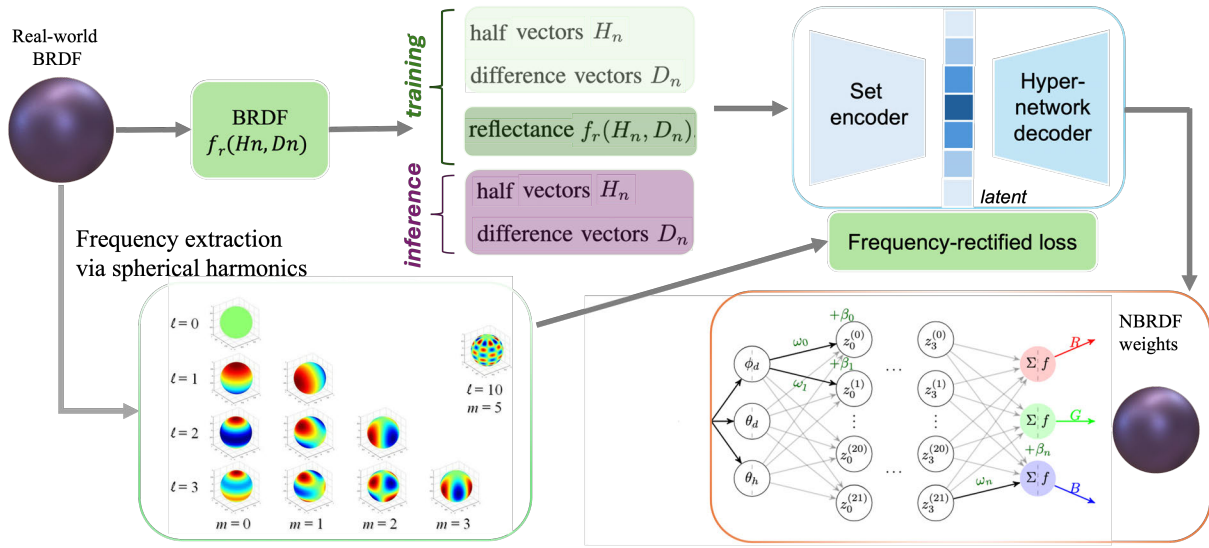University of Cambridge

Fig. 1. Overview of FreNBRDF architecture.

ABSTRACT

Accurate material modeling is crucial for achieving photorealistic rendering, bridging the gap between computer-generated imagery and real-world photographs. While traditional approaches rely on tabulated BRDF data, recent work has shifted towards implicit neural representations, which offer compact and flexible frameworks for a range of tasks. However, their behavior in the frequency domain remains poorly understood. To address this, we introduce *FreNBRDF*, a frequency-rectified neural material representation. By leveraging spherical harmonics, we integrate frequency-domain considerations into neural BRDF modeling. We propose a novel *frequency-rectified loss*, derived from a frequency analysis of neural materials, and incorporate it into a generalizable and adaptive reconstruction and editing pipeline. This framework enhances fidelity, adaptability, and efficiency. Extensive experiments demonstrate that FreNBRDF improves the accuracy and robustness of material appearance reconstruction and editing compared to state-of-the-art baselines, enabling more structured and interpretable downstream tasks and applications.

Index Terms— Appearance modeling, frequency-aware methods, material reconstruction, material editing

1. INTRODUCTION

Material properties play a crucial role in visual computing, serving as a fundamental component in applications such as rendering, augmented reality, and scene understanding [1]. This is usually realized through the modeling and reconstruction of the *bidirectional reflectance distribution functions (BRDFs)* [2], which describe the relationship between the incident and outgoing radiances for a specific material. By capturing the complex interactions of light with different surfaces, material representations enhance the realism and fidelity of synthesized images, improving the overall visual quality in various computational applications.

Data-driven BRDF models [3], which map spatial coordinates to reflected light distributions, have demonstrated high fidelity in capturing complex material appearances. However, their inherently large data size poses significant challenges for downstream tasks such as material reconstruction, editing, storage, and real-time rendering. Efficiently representing

---

[†]: Equal contribution.

and reconstructing BRDF data still remains a critical issue.

Implicit neural BRDF models (*e.g.*, *NBRDFs* [4, 1, 5]) offer a promising solution to these challenges by incorporating neural networks into the BRDF modeling pipeline, providing a more scalable and adaptive solution for material representation. Based on NBRDF, recent research has explored leveraging latent space representations through an encoder-decoder architecture [6]. This approach seeks to reconstruct BRDFs from a compressed latent space, reducing memory requirements while maintaining high reconstruction fidelity.

However, the behavior of material representations in the frequency domain remains insufficiently explored. To address this gap, we propose *FreNBRDF*, a frequency-rectified neural material representation. By leveraging spherical harmonics, we integrate frequency rectification [7] into the NBRDF framework and introduce a novel *frequency-rectified loss* to achieve a more structured and accurate representation of material appearance. The primary contributions of this work are:

- A method for extracting frequency information from neural materials using spherical harmonics; and
- A generalizable and adaptive material reconstruction and editing framework based on an autoencoder architecture, incorporating frequency rectification and achieving state-of-the-art performance.

2. RELATED WORK

Material acquisition Gonio-photometers [8] are widely used for measuring retro-reflection, enabling precise characterization of material appearance. Using this technique, RGL [9] captured 62 materials, including anisotropic ones. In contrast, image-based measurement devices [10] were used to construct the MERL dataset [3], which consists of 100 isotropic materials. Similarly, digital consumer cameras have been employed for texture acquisition [11], forming the *bidirectional texture function database Bonn (BTFDBB)* using 151 such cameras mounted on a structured rack.

Material modeling *Bidirectional reflectance distribution functions (BRDFs)* [2] are widely adopted for material modeling. Early BRDF models [12, 13, 14] introduced analytical expressions derived from empirical observations. Other models [15, 16, 17] incorporate physical scattering principles while maintaining artist-friendly parameterization. These models offer a balance between realism and efficiency, as their limited set of tunable parameters can be fitted to measured material data [17], making them computationally efficient in terms of both time and memory. However, due to inherent model approximations, many analytical BRDFs struggle to capture complex reflectance behaviors, particularly for highly detailed or anisotropic materials [4].

Neural BRDFs Data-driven material representations (*e.g.*, MERL [3]) produce highly realistic renderings compared to analytical models. However, their large data size presents a significant challenge for real-world applications. To address this, compression techniques such as dimensionality reduction [18] or neural network-based compression [4, 6] are commonly used. Among these, *neural BRDFs (NBRDFs)* [4] offer a compelling balance of high fidelity and low memory demand, making them an efficient latent representation for various tasks. Built upon this, recent research has introduced a set encoder hypernetwork [6] that enables generalizable and adaptive BRDF reconstruction from sparse samples. This approach is designed to handle unseen data while accommodating varying sample sizes, making it a flexible and scalable solution. Building on this work, we further explore neural BRDF representations within the frequency domain.

Frequency rectification FrePolad [7] utilizes spherical harmonics [19] to extract frequency information from point clouds, improving the quality and diversity of point cloud generation while maintaining high computational efficiency. Inspired by this approach, we integrate frequency information into the NBRDF representation, aiming to enhance accuracy in NBRDF modeling, reconstruction, and editing.

3. METHOD

3.1. NBRDF autoencoder pipeline

Under Rusinkiewicz reparameterization of BRDFs [20], we represent the incoming and outgoing directions using the half H and difference D vectors or their spherical coordinates θ_H, ϕ_H and the difference vector θ_D, ϕ_D, respectively. Note that for isotropic materials, the BRDFs are independent of ϕ_D. Therefore, a BRDF can be expressed as either $f_r(H, D)$ or $f_r(\theta_H, \theta_D, \phi_H)$.

Inspired by prior work [4, 6, 5], we first represent BRDFs via lightweight neural fields called *NBRDFs* [4] that map the half H_n and difference vectors D_n to reflectance values $f_r(H_n, D_n)$. To facilitate NBRDF reconstruction and editing, our autoencoder-based pipeline trains a pair of encoder and decoder to capture a lower dimensional space of the weights of NBRDFs. During inference, the model accepts queries in terms of (H, D) coordinate and returns the reflectance values at that coordinate. Moreover, the set encoder provides low-dimensional embeddings of neural materials, enabling material editing through interpolation. By linearly interpolating between the embeddings of different materials, we can reconstruct a range of novel appearances. We illustrate this autoencoder architecture in Fig. 1.

For the network, we adopt a set encoder [21] with permutation invariance and flexibility of input size. It takes an arbitrary set of samples as input, which is the concatenation of BRDF values and coordinates, containing four fully connected layers with two hidden layers of 128 hidden neurons and ReLU activation function. The reconstruction loss $\mathcal{L}_{\text{rec}}(f_r, f_r')$ between two NBRDFs is defined to be the sum of the L1 loss between samples of the two underlying BRDFs

and the two regularization terms for NBRDF weights w and latent embeddings z:

$$\mathcal{L}_{\text{rec}}(f_r, f'_r) := \frac{1}{|P|} \sum_{i=1}^{|P|} |(f_r(H_i, D_i) - f'_r(H_i, D_i)) \cos \theta_i|$$
$$+ \lambda_1 \sum_{i=1}^{W} w_i^2 + \lambda_2 \sum_{j=1}^{Z} z_j^2, \quad (1)$$

where P is the predefined set of indices for samples, θ_i is the angle between the incoming light direction and the normal of the surface, and λ_1 and λ_2 are regularization coefficients.

Following previous work [18], we also adopt the pre-processing technique of log-relative mapping for BRDFs:

$$f_r \mapsto \ln \left(\frac{f_r + \epsilon}{f_{\text{ref}} + \epsilon} \right) \quad (2)$$

where the reference value f_{ref} is the median BRDF value and ϵ is a small constant to avoid division or logarithm of zero.

3.2. Frequency Recitification

We observe that the naive NBRDF autoencoder pipeline described above lacks the frequency information between the two NBRDFs, which might help the learning of NBRDF weight distribution [7]. To extract frequency information from BRDFs, we apply spherical harmonic transformation [19, 7]. Note that the spherical harmonics require continuous functions on the unit sphere S^2. Our first problem is that the BRDF $f_r(\theta_H, \theta_D, \phi_H)$ is not a function on S^2. We address this by fixing the third argument ϕ_H to some value α, and the function is thus defined on S^2:

$$f_r(\theta, \phi) := f_r(\theta_H, \theta_D, \phi_H = \alpha). \quad (3)$$

We can then apply the technique multiple times for different values of ϕ_H and average the result.

Another problem is that the given MERL dataset [3] only provides BRDF values at discrete sample positions P, but we need a continuous function. To overcome this, we obtain the BRDF values at an arbitrary position (θ, ϕ) by interpolating the values at its k nearest neighbors $P_k(\theta, \phi)$ in the sample positions P with weights w_i:

$$f_r(\theta, \phi) := \sum_{i \in P_k(\theta, \phi)} w_i f_r(\theta_i, \phi_i). \quad (4)$$

The k nearest neighbors (θ_i, ϕ_i) of (θ, ϕ) are determined through their distances d_i to the points (θ, ϕ):

$$d_i = \sqrt{2 - 2 \left[\sin \theta \sin \theta_i \cos(\phi - \phi_i) + \cos \theta \cos \theta_i \right]}. \quad (5)$$

For the choice of weights w_i, since closer points should have larger weights, $\{w_i\}_i$ should be a decreasing sequence on d_i.

Consequently, a suitable candidate is the normalized Gaussian function with standard deviation σ:

$$w'_i := e^{-\frac{d_i^2}{2\sigma^2}}; \quad (6)$$

$$w_i := \frac{w'_i}{\sum_j w'_j}. \quad (7)$$

After we obtain BRDFs expressed as continuous functions on the unit sphere S^2, we can further leverage spherical harmonics to express them as a linear combination of orthonormal base functions $G : S^2 \to \mathbb{C}$ of degrees l and orders m:

$$f_r(\theta, \varphi) = \sum_{l=0}^{\infty} \sum_{m=-l}^{l} c_{l,m} G_{l,m}(\theta, \varphi); \quad (8)$$

$$c_{l,m} = \int_0^{2\pi} \int_0^{\pi} f_r(\theta, \phi) \overline{G_{l,m}(\theta, \phi)} \sin \theta \, d\theta d\phi. \quad (9)$$

Note that BRDFs have three channels (RGB). Therefore, we apply the above method to each channel separately, producing the frequency coefficients $c_{l,m} \in \mathbb{R}^3$. The key insight here is that these frequency coefficients now contain the extracted frequency information at each degree l and order m. Therefore, we can define a *frequency-rectified loss* on BRDFs based on the mean squared error of frequency coefficients

$$\mathcal{L}_{\text{fre}}(f_r, f'_r) := \frac{1}{|P|} \sum_{i=1}^{|P|} \left\| c_{l,m} - c'_{l,m} \right\|^2 \quad (10)$$

and consequently, we can incorporate this loss into the reconstruction loss Eq. (1):

$$\mathcal{L}(f_r, f'_r) := \mathcal{L}_{\text{rec}}(f_r, f'_r) + \eta \mathcal{L}_{\text{fre}}(f_r, f'_r), \quad (11)$$

where $\eta \in \mathbb{R}$ is the hyperparameter controlling the strength of frequency rectification and $c_{l,m}$ and $c'_{l,m}$ are the frequency coefficients for f_r and f'_r, respectively. With the help of frequency information, our pipeline is able to better learn the NBRDF weight distribution, enabling better reconstruction and editing tasks as demonstrated in Sec. 4.

4. EXPERIMENTS

4.1. Dataset

The MERL dataset [3] is used in this study for its diversity and data-driven nature, making it suitable for both statistical and neural-network-based methods. It contains 100 measured real-world materials. Each BRDF is represented as a $90 \times 90 \times 180 \times 3$ floating-point array, mapping uniformly sampled input angles $(\theta_H, \theta_D, \phi_D)$ under Rusinkiewicz reparametrization [20] to reflectance values in $\mathbb{R}^3$.
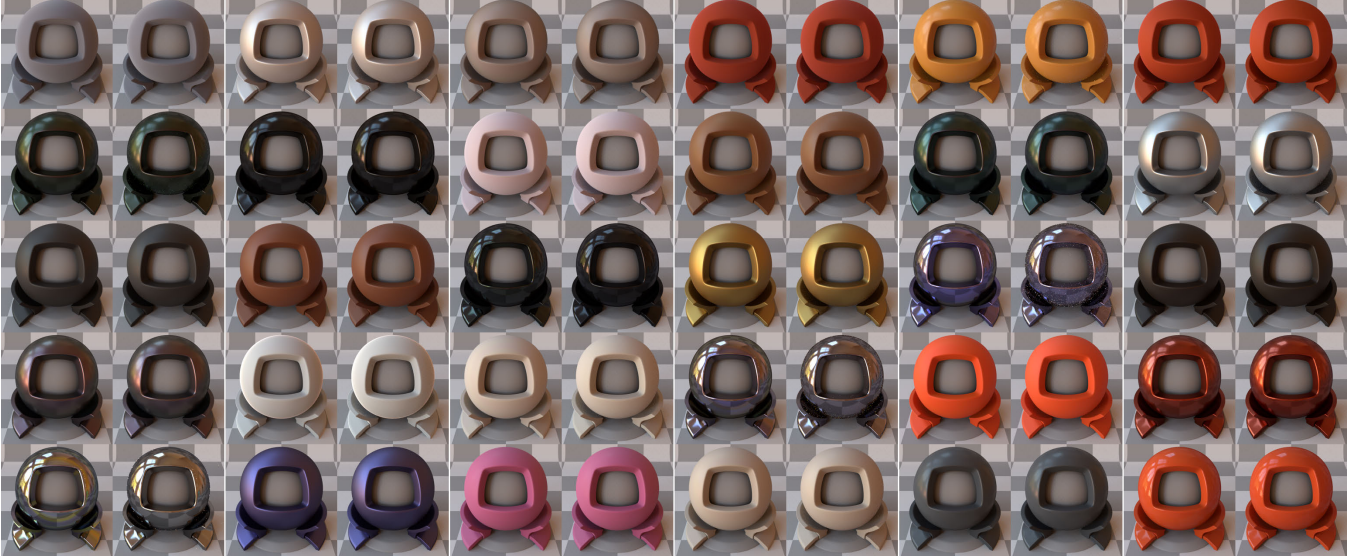
Fig. 2. FreNBRDF reconstructs 30 MERL materials [3] with high quality, indicating that FreNBRDF effectively learns the material distribution (ground truths to the left and the reconstructed material to the right).

4.2. Training and testing procedures

The dataset is divided into training, validation, and testing sets in a 70%-10%-20% split. We use the Adam optimizer [22], a first-order gradient-based method for optimizing stochastic objective functions.

During training, the specified losses are reported at each epoch, and optimal hyperparameters are selected based on performance on the validation set. Model performance is then evaluated on the hold-out test set using a range of quantitative metrics introduced in Sec. 4.3.

4.3. Metrics

To evaluate the performance of material reconstruction and editing, we report the frequency-rectified loss (Eq. (10)) accessing the frequency compliance. We also report the following three rendering-based metrics assessing the perceptual similarity and reconstruction quality between the two images $I_1, I_2 \colon \{1, 2, \ldots, w\} \times \{1, 2, \ldots, h\} \to [0, 1]^3$, where w, h are the width and height of the images:

- Root mean squared error (RMSE). RMSE checks if pixel values at the same coordinates match:

$$\mathcal{L}_{\text{RMSE}}(I_1, I_2) \coloneqq \sqrt{\frac{1}{wh} \sum_{i=1}^{w} \sum_{j=1}^{h} (I_1(i,j) - I_2(i,j))^2}. \tag{12}$$

Note that RMSE depends strongly on the image intensity scaling. RMSE aims for a lower value.

- Peak signal-to-noise ratio (PSNR). PSNR is the scaled mean squared error (MSE). PSNR measures the image reconstruction quality and aims for higher values. Given the maximum pixel value p, PSNR is defined as

$$\mathcal{L}_{\text{PSNR}}(I_1, I_2) \coloneqq 10 \log_{10} \frac{p^2}{\mathcal{L}_{\text{RMSE}}^2(I_1, I_2)}. \tag{13}$$

- Structural similarity index measure (SSIM) [23]. SSIM is a perception-based metric that measures the perceptual similarity between the two images, which aims for higher values for better performance. SSIM is computed from the luminance $l(I_1, I_2)$, contrast $c(I_1, I_2)$, and structure $s(I_1, I_2)$ of the two images with exponential weights $a, b, c > 0$:

$$\mathcal{L}_{\text{SSIM}}(I_1, I_2) \coloneqq l^a(I_1, I_2)c^b(I_1, I_2)s^c(I_1, I_2). \tag{14}$$

4.4. Material reconstruction

We present 30 reconstructed materials rendered under consistent scene and lighting conditions in Fig. 2. The results demonstrate that FreNBRDF effectively learns the material distribution and produces high-quality, faithful reconstructions. In Tab. 1, we compare the performance of FreNBRDF on the material reconstruction task with two state-of-the-art baselines: the method of Gokbudak *et al.* [6] and a naive NBRDF [4] reconstruction pipeline, as described in Sec. 3.1, without frequency rectification. From the results, we can see that FreNBRDF outperforms both baselines across most metrics evaluating frequency compliance, rendering quality, and visual similarity, confirming the effectiveness of our proposed approach. Note that the higher RMSE score for FreNBRDF is likely due to its reconstruction loss (Eq. (11)) being designed to enforce consistency in both the spatial and frequency domains.

Metrics	[6]	NBRDF [4]	FreNBRDF (ours)
RMSE$\times 10^2$ ($\downarrow$)	6.89	**6.60**	6.74
PSNR ($\uparrow$)	26.3	29.2	**29.9**
SSIM$\times 10$ ($\uparrow$)	9.26	9.50	**9.88**
$\mathcal{L}_{\text{fre}} \times 10^3$ ($\downarrow$)	6.74	6.80	**0.23**

Table 1. Quantitative comparison on material reconstruction against state-of-the-art baselines. FreNBRDF achieves superior performance, showing its effectiveness.

Metrics	[6]	NBRDF [4]	FreNBRDF (ours)
RMSE$\times 10^2$ ($\downarrow$)	8.42	7.63	**6.92**
PSNR ($\uparrow$)	22.4	27.6	**30.1**
SSIM$\times 10$ ($\uparrow$)	9.13	9.42	**9.82**
$\mathcal{L}_{\text{fre}} \times 10^3$ ($\downarrow$)	6.72	6.80	**0.22**

Table 2. Quantitative comparison on material editing with two state-of-the-art baselines. Materials represented by FreNBRDF exhibit significantly higher quality compared to the two baselines, indicating that FreNBRDF effectively learns the distribution of neural materials.

4.5. Material editing

Our pipeline provides a low-dimensional space of neural materials, enabling material editing by linearly interpolating between embeddings of different materials. We compare different models on this task. The ground truth can be obtained by directly linearly interpolating the MERL materials [3].

Figure 3 illustrates interpolations between five pairs of MERL materials where each row represents one interpolation. The smooth transitions between the two endpoints demonstrate the capability of our FreNBRDF as a robust and effective implicit neural representation for materials. We also report the relevant metrics in Tab. 2, computed over 2000 randomly interpolated materials. The results show that materials represented by FreNBRDF exhibit consistently higher quality compared to the two baselines. Compared to the reconstruction results in Tab. 1, the interpolated materials produced by the two baselines show degraded performance, while those generated by FreNBRDF maintain similar quality. This indicates that FreNBRDF effectively captures the underlying distribution of neural materials.

4.6. Further analysis

We further visualize the sample-wise performance of the naive NBRDF [4] reconstruction pipeline and FreNBRDF with frequency rectification in Figs. 4 and 5, respectively, with the mean (solid line) and variance (dashed line) indicated. This visualization reveals overall statistical trends and helps identify outliers or failure cases, providing deeper insight into each model's behavior. The results show that

Fig. 3. Linearly interpolation between embeddings of five pairs of MERL materials (each row is an interpolation). From left to right, the interpolation weights are 0.0, 0.2, 0.4, 0.6, 0.8, 1.0. The smooth transitions between the two endpoints demonstrate the capability of our FreNBRDF as a robust and effective implicit neural representation for materials.


(a) RMSE　　　(b) PSNR　　　(c) SSIM
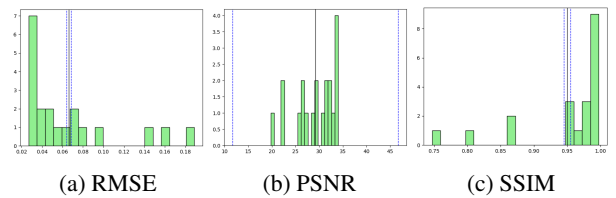
Fig. 4. Sample-wise performance of the naive NBRDF reconstruction with mean (solid) and variance (dashed line).

FreNBRDF effectively reduces frequency domain discrepancies while maintaining comparable qualitative and quantitative performance. This underscores the potential of our method and suggests promising directions for future research in frequency-aware material modeling.

5. CONCLUSION AND FUTURE WORK

In this work, we propose FreNBRDF, a frequency-rectified neural material representation. Building on this representation, we develop a material reconstruction and editing pipeline based on an autoencoder architecture, incorporating a novel *frequency-rectified loss* to enforce accuracy in the frequency domain. We evaluate our method against state-of-the-art baselines using both qualitative and quantitative metrics, with FreNBRDF consistently outperforming competing approaches. By integrating frequency information, FreNBRDF has the potential to unlock novel techniques for

(a) RMSE   (b) PSNR   (c) SSIM
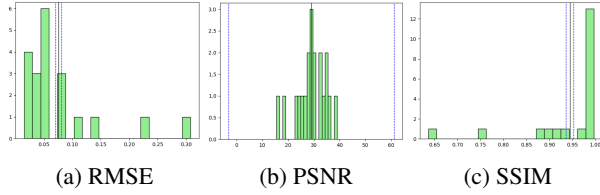
Fig. 5. Sample-wise performance of FreNBRDF on material reconstruction, with mean (solid) and variance (dashed line).

refining material details.

Promising directions for future work include extending the approach to more complex materials, such as anisotropic BRDFs, spatially varying BRDFs, and physically-based materials. We also hope this work contributes to future research and applications, including game development, virtual environments, and simulation systems, where realistic material representation is crucial for visual accuracy and immersion.

6. REFERENCES

[1] Chenliang Zhou, Zheyuan Hu, Alejandro Sztrajman, Yancheng Cai, Yaru Liu, and Cengiz Oztireli, "Neumadiff: Neural material synthesis via hyperdiffusion," 2024.

[2] Mislene da Silva Nunes, Fernando Melo Nascimento, Gastão Florêncio Miranda Jr., and Beatriz Trinchão Andrade, "Techniques for brdf evaluation," *The Visual Computer*, vol. 38, pp. 573 – 589, 2021.

[3] W. Matusik, H. Pfister, M. Brand, and L. McMillan, "A data-driven reflectance model," *ACM Transactions on Graphics (TOG)*, vol. 22, no. 3, pp. 759–769, July 2003.

[4] Alejandro Sztrajman, Gilles Rainer, Tobias Ritschel, and Tim Weyrich, "Neural brdf representation and importance sampling," *Computer Graphics Forum*, 2021.

[5] Chenliang Zhou, Alejandro Sztrajman, Gilles Rainer, Fangcheng Zhong, Fazilet Gokbudak, Zhilin Guo, Weihao Xia, Rafal Mantiuk, and Cengiz Oztireli, "Physically based neural bidirectional reflectance distribution function," *arXiv preprint arXiv:2411.02347*, 2024.

[6] Fazilet Gokbudak, Alejandro Sztrajman, Chenliang Zhou, Fangcheng Zhong, Rafal Mantiuk, and Cengiz Oztireli, "Hypernetworks for generalizable brdf representation," *The 18th European Conference on Computer Vision (ECCV)*, 2024.

[7] Chenliang Zhou, Fangcheng Zhong, Param Hanji, Zhilin Guo, Kyle Fogarty, Alejandro Sztrajman, Hongyun Gao, and Cengiz Oztireli, "Frepolad: Frequency-rectified point latent diffusion for point cloud generation," in *ECCV 2024*, 2024.

[8] PAB Advanced Technologies Ltd., "Pab pgii goniophotometer," 2018, Accessed: 2018-01-09.

[9] Jonathan Dupuy and Wenzel Jakob, "An adaptive parameterization for efficient material acquisition and rendering," *Transactions on Graphics (Proceedings of SIGGRAPH Asia)*, vol. 37, no. 6, pp. 274:1–274:18, Nov. 2018.

[10] Stephen R. Marschner, Stephen H. Westin, Eric P. F. Lafortune, and Kenneth E. Torrance, "Image-based bidirectional reflectance distribution function measurement," *Appl. Opt.*, vol. 39, no. 16, pp. 2592–2600, Jun 2000.

[11] Christopher Schwartz, Ralf Sarlette, Michael Weinmann, Martin Rump, and Reinhard Klein, "Design and implementation of practical bidirectional texture function measurement devices focusing on the developments at the university of bonn," *Sensors*, vol. 14, no. 5, 2014.

[12] Bui Tuong Phong, "Illumination for computer generated pictures," *Commun. ACM*, vol. 18, no. 6, pp. 311–317, jun 1975.

[13] Eric P. F. Lafortune, Sing-Choong Foo, Kenneth E. Torrance, and Donald P. Greenberg, "Non-linear approximation of reflectance functions," in *Proceedings of the 24th Annual Conference on Computer Graphics and Interactive Techniques*, USA, 1997, SIGGRAPH '97, p. 117–126, ACM Press/Addison-Wesley Publishing Co.

[14] Gregory J. Ward, "Measuring and modeling anisotropic reflection," *SIGGRAPH Comput. Graph.*, vol. 26, no. 2, pp. 265–272, jul 1992.

[15] R. L. Cook and K. E. Torrance, "A reflectance model for computer graphics," *ACM Trans. Graph.*, vol. 1, no. 1, pp. 7–24, jan 1982.

[16] Bruce Walter, Stephen R. Marschner, Hongsong Li, and Kenneth E. Torrance, "Microfacet models for refraction through rough surfaces," in *Proceedings of the 18th Eurographics Conference on Rendering Techniques*, Goslar, DEU, 2007, EGSR'07, p. 195–206, Eurographics Association.

[17] Brent Burley, "Physically-based shading at disney," *SIGGRAPH Comput. Graph.*, 2012.

[18] Jannik Boll Nielsen, Henrik Wann Jensen, and Ravi Ramamoorthi, "On optimal, minimal brdf sampling for reflectance acquisition," *ACM Transactions on Graphics (TOG)*, vol. 34, no. 6, pp. 186:1–186:11, November 2015.

[19] Boris Bonev, Thorsten Kurth, Christian Hundt, Jaideep Pathak, Maximilian Baust, Karthik Kashinath, and Anima Anandkumar, "Spherical fourier neural operators: Learning stable dynamics on the sphere," 2023.

[20] Szymon M. Rusinkiewicz, "A new change of variables for efficient brdf representation," in *Rendering Techniques '98*, George Drettakis and Nelson Max, Eds., Vienna, 1998, pp. 11–22, Springer Vienna.

[21] Manzil Zaheer, Satwik Kottur, Siamak Ravanbhakhsh, Barnabás Póczos, Ruslan Salakhutdinov, and Alexander J Smola, "Deep sets," in *Proceedings of the 31st International Conference on Neural Information Processing Systems*, Red Hook, NY, USA, 2017, NIPS'17, p. 3394–3404, Curran Associates Inc.

[22] Diederik P. Kingma and Jimmy Ba, "Adam: A method for stochastic optimization," *CoRR*, vol. abs/1412.6980, 2014.

[23] Zhou Wang, A.C. Bovik, H.R. Sheikh, and E.P. Simoncelli, "Image quality assessment: from error visibility to structural similarity," *IEEE Transactions on Image Processing*, vol. 13, no. 4, pp. 600–612, 2004.